

COSMOLOGICAL PARAMETER ESTIMATION FROM LARGE-SCALE STRUCTURE DEEP LEARNING

SHUYANG PAN, MIAOXIN LIU,¹ JAIME FORERO-ROMERO,² CRISTIANO G. SABIU,³ ZHIGANG LI,⁴ HAITAO MIAO,¹ AND
XIAO-DONG LI ^{*1}

¹*School of Physics and Astronomy, Sun Yat-Sen University, Guangzhou 510297, P.R.China*

²*Departamento de Física, Universidad de los Andes, Cra. 1 No. 18A-10 Edificio Ip, CP 111711, Bogotá, Colombia*

³*Department of Astronomy, Yonsei University, Seoul, Korea*

⁴*College of Physics and Electronic Engineering, Nanyang Normal University, Nanyang, Henan, 473061, China*

(Received November 6, 2017; Revised November 27, 2017; Accepted March 13, 2024)

Submitted to ApJ

ABSTRACT

We propose a light-weight deep convolutional neural network (CNN) to estimate the cosmological parameters from simulated 3-dimensional dark matter distributions with high accuracy. The training set is based on 465 realizations of a cubic box with a side length of $256 h^{-1}$ Mpc, sampled with 128^3 particles interpolated over a cubic grid of 128^3 voxels. These volumes have cosmological parameters varying within the flat Λ CDM parameter space of $0.16 \leq \Omega_m \leq 0.46$ and $2.0 \leq 10^9 A_s \leq 2.3$. The neural network takes as an input cubes with 32^3 voxels and has three convolution layers, three dense layers, together with some batch normalization and pooling layers. In the final predictions from the network we find a 2.5% bias on the primordial amplitude σ_8 that can not easily be resolved by continued training. We correct this bias to obtain unprecedented accuracy in the cosmological parameter estimation with statistical uncertainties of $\delta\Omega_m=0.0015$ and $\delta\sigma_8=0.0029$, which are several times better than the results of previous CNN works. Compared with a 2-point analysis method using clustering region of 0-130 and 10-130 h^{-1} Mpc, the CNN constraints are several times and an order of magnitude more precise, respectively. Finally, we conduct preliminary checks of the error-tolerance abilities of the neural network, and find that it exhibits robustness against smoothing, masking, random noise, global variation, rotation, reflection, and simulation resolution. Those effects are well understood in typical clustering analysis, but had not been tested before for the CNN approach. Our work shows that CNN can be more promising than people expected in deriving tight cosmological constraints from the cosmic large scale structure.

Keywords: large-scale structure of Universe — dark energy — cosmological parameters

* Corresponding Author: lixiaod25@mail.sysu.edu.cn

1. INTRODUCTION

The current standard model of cosmology has been highly successful at describing the Universe on large scales. From the anisotropic temperature fluctuations in the cosmic microwave background (CMB) to the late time clustering of galaxies, the vacuum energy dominated cold dark matter model (Λ CDM) (Weinberg 1989; Peebles & Ratra 2003; Miao et al. 2011) fits the data surprisingly well (Riess et al. 1998; Perlmutter et al. 1999; Weinberg et al. 2013; Ade et al. 2016; Alam et al. 2017). For cosmologists, one main task would be to precisely estimate the parameters of the Universe, such as the dark matter ratio Ω_m , the local expansion rate H_0 , the amplitude and index of the primordial fluctuation A_s and n_s , the dark energy equation of state w together with its time dependence w_a , and so on.

The spatial distribution of galaxies on scales of a few hundred Megaparsecs (Mpc) forms a distinct, very complicated filamentary motif known as the ‘cosmic web’ (Bardeen et al. 1986; de Lapparent et al. 1986; Huchra et al. 2012; Tegmark et al. 2004; Guzzo et al. 2014). The distribution and clustering properties of galaxies in the cosmic web encodes information on the expansion and the structure growth history of the Universe. In the next decades, several large scale surveys (e.g., DESI¹, EUCLID², LSST³, WFIRST⁴) will begin operations to map out an unprecedented large volume of the Universe with extraordinary precision. It becomes essential to develop powerful tools that can comprehensively and reliably infer the cosmological parameters from large scale structure (LSS) data.

Currently, the most widely-adopted LSS data mining methods is still the 2-point correlation function (2pCF) or power spectrum measurements, which are sensitive to the geometric and structure growth history of the Universe (Kaiser 1987; Ballinger et al. 1996; Eisenstein et al. 1998; Blake & Glazebrook 2003; Seo & Eisenstein 2003). These methods have achieved tremendous success when applied to a series of galaxy redshift surveys such as the 2-degree Field Galaxy Redshift Survey (2dFGRS; Colless et al. (2003)), the 6-degree Field Galaxy Survey (6dFGS; Beutler et al. (2011)), the WiggleZ survey (Blake et al. (2011b,a)), and the Sloan Digital Sky Survey (SDSS; York et al. (2000); Eisenstein et al. (2005); Percival et al. (2007); Anderson et al. (2012); Sánchez et al. (2012, 2013); Anderson et al. (2014); Samushia

et al. (2014); Ross et al. (2015); Beutler et al. (2016); Sánchez et al. (2016); Alam et al. (2017); Chuang et al. (2017). The main caveat of this method is that, the distribution of structures and their velocities on scales of $\lesssim 40h^{-1}$ Mpc are highly affected by the non-linear processes, making it difficult to conduct a comparison between observations and theories.

Ongoing research seeks to utilise LSS data on non-linear scales or beyond the usual 2nd order spatial statistics. The next order correlation function, the 3-point correlation function, has been shown to add cosmological constraints beyond the 2pCF (Slepian et al. 2017) and it has also shown promise in constraining modified gravity models (Sabiou et al. 2016). The 4-point function may also lead to improved constraints if it can be modelled correctly (Sabiou et al. 2019).

Some other tests include the proposal to use the apparent stretching of cosmic voids as a probe of geometry (Ryden 1995; Lavaux & Wandelt 2012); the redshift invariance of the comoving scale information in the LSS to probe the expansion history (Li et al. 2014; Li et al. 2017); the symmetry properties of galaxy pairs to conduct an Alcock-Paczynski (AP) tests (Alcock & Paczyński 1979; Marinoni & Buzzi 2010); the redshift-dependent property of the AP effect to overcome the effect of redshift space distortion (RSD) (Li et al. 2014; Li et al. 2015) to successfully derive tight dark energy constraints from the SDSS galaxies (Li et al. 2014, 2018, 2019b; Zhang et al. 2019b). Recently, Fang et al. (2019) applied the so-called β -skeleton statistics to study LSS and proposed its application for cosmological analysis; Ramanah et al. (2019b) proposed to use the large-scale Bayesian inference framework to constrain parameters via the AP test.

To summarize, there are many alternative ideas and concepts that have been used proposed and used to extract information from the LSS, and one may refer to Weinberg et al. (2013) and the references therein for a more complete overview.

While cosmologists have obtained prominent information about the physics of the Universe via the current statistical methods, due to the extreme sophistication of the cosmic web we are still far from having a statistical method to comprehensively explore the overwhelming information encoded in the cosmic LSS. Fortunately, recent developments in machine learning techniques may allow us to capture and extract more cosmological information from the complex LSS data.

Machine learning techniques, especially the deep learning algorithms based on deep neural networks, are becoming a mainstream toolkit for modeling the relationship between complex data and the underlying

¹ <https://desi.lbl.gov/>

² <http://sci.esa.int/euclid/>

³ <https://www.lsst.org/>

⁴ <https://wfirst.gsfc.nasa.gov/>

variables that it corresponds to. They make it possible to extract and analyze features contained within the data, which can not be easily identified via traditional methods of scientific research ⁵. Recently, machine learning techniques have been applied to many sub-fields of cosmology, including weak gravitational lensing (Schmelzle et al. 2017; Gupta et al. 2018; Springer et al. 2018; Fluri et al. 2019; Jeffrey et al. 2019; Merten et al. 2019; Peel et al. 2019; Tewes et al. 2019), the cosmic microwave background (Caldeira et al. 2018; Rodriguez et al. 2018; Perraudin et al. 2019; Mnchmeyer & Smith 2019; Mishra et al. 2019), the large scale structure (Lucie-Smith et al. 2018; Modi et al. 2018; Berger & Stein 2019; He et al. 2019; Lucie-Smith et al. 2019; Pfeffer et al. 2019; Ramanah et al. 2019a; Trster et al. 2019; Zhang et al. 2019a), gravitational waves (Dreissigacker et al. 2019; Gebhard et al. 2019), cosmic reionization (La Plante & Ntampaka 2018; Gillet et al. 2019; Hassan et al. 2019b; Chardin et al. 2019; Hassan et al. 2019a), supernovae (Lochner et al. 2016; Moss 2018; Ishida et al. 2019; Li et al. 2019a; Muthukrishna et al. 2019). For more details, one can refer to Mehta et al. (2019); Jennings et al. (2019); Carleo et al. (2019); Ntampaka et al. (2019) and the references therein.

In a pioneering work, Ravanbakhsh et al. (2017) presented a CNN (convolutional neural network) to infer cosmological parameters from simulated 3-dimensional dark matter density fields. They were able to constraint Ω_m and the matter over-density variance σ_8 , finding that the machine learning techniques can outperform the traditional 2pCF statistics. Mathuriya et al. (2018) presented a more sophisticated framework, which can achieve synchronous parallel calculation on tens of thousands of nodes, and simultaneously predict Ω_m , σ_8 , and the primordial power spectrum index n_s .

In this work we build upon those previous studies to explore a new deep learning architecture and perform new tests to study the LSS. We show that it is possible to constrain Ω_m and σ_8 using 32^3 voxels only as an input, a small number compared to the larger sizes of 64^3 and 128^3 used by Ravanbakhsh et al. (2017) and Mathuriya et al. (2018), respectively. Compared with Ravanbakhsh et al. (2017), we achieve an order of magnitude better constraints on the parameters, while the architecture we propose is also simpler than the ones suggested in those two works. Finally, although CNNs are able to achieving state-of-the-art performance on many tasks, some recent studies revealed that they can also be easily fooled ? by either giving wrong prediction

from minor changes in the inputs or giving seemingly correct values for unreasonable inputs. Here we also test for error-tolerance abilities of the neural network to different effects that are well understood in traditional clustering analysis (smoothing, masking, random noise, global variation, rotation, reflection, simulation resolution) but have not been fully explored in the context of predicting cosmological parameters using CNNs.

This paper is structured as follows. In Section 2 we introduce the samples used for the training and testing, while the Section 3 we explain the architecture of our neural network. The results are presented in Section 4. We conclude in Section 5 by discussing the future of the technique and its caveats.

2. DATA

The training and testing samples are created with the COMoving Lagrangian Acceleration (COLA) code (Tassev et al. 2013; Koda et al. 2016), which is designed as a mixture of N-body and perturbation theory to simulations with fast speed and good accuracy. We choose COLA because it is hundreds of times faster than N-body simulations, while keeping a good accuracy in generating structures on non-linear scales.

We change two cosmological parameters in our simulations, the fraction of matter, Ω_m , and the amplitude of the primordial power spectrum, A_s . Values of the other parameters are taken as $\Omega_b = 0.048206$, $h = 0.6777$, $n_s = 0.96$, the same as the MultiDark Planck N-body simulations (Klypin et al. 2016).

We vary the values of Ω_m and A_s on a 31×15 grid, i.e. $0.16 \leq \Omega_m \leq 0.46$ with step size 0.01, and $2.0 \leq 10^9 A_s \leq 2.3$ with step size 0.02. This parameter space is centered around the Planck 2015 best fit cosmology (Ade et al. 2016) ⁶. This leads to a varying σ_8 in the range of 0.4-1.1.

For all samples, we run a simulation with 128^3 particles, in a $(256 h^{-1} \text{Mpc})^3$ box, using 40 timesteps. We output the normalized density field,

$$\delta\rho(\mathbf{x}) \equiv \frac{\rho(\mathbf{x})}{\bar{\rho}}, \quad (1)$$

on a grid with 128^3 voxels at redshift $z = 0$,

To train the neural network we generate 31×15 samples (i.e. boxes) – one sample for an individual cosmology. The simulation adopted the second-order Lagrangian perturbation theory (2LPT) initial conditions at $z_i = 39$. Each cosmology is evolved from initial con-

⁵ <https://www.oreilly.com/ideas/a-look-at-deep-learning-for-science>

⁶ Planck 2015 (TT,TE,EE+lowP+lensing) gives $\Omega_m = 0.3121 \pm 0.0087$, $10^9 A_s = 2.13 \pm 0.053$, $\sigma_8 = 0.8150 \pm 0.0087$ in the Λ CDM framework.

ditions with different random seeds and thus different distributions of large scale power, so that our neural network can capture the cosmic variance.

To test the neural network we generated two sets of testing samples:

- The “single-cosmology” testing samples, for which we generated 500 samples sharing the same cosmology $(\Omega_m, \sigma_8) = (0.3072, 0.8228)$. This allows us to validate the statistical error of the neural network predictions.
- The “multi-cosmology” samples, wherein we have 31×15 samples, using different cosmologies (on the same grid of the testing sample cosmology grid). The multi-cosmology set allows us to validate the accuracy of the parameter estimation in the whole parameter space.

The testing samples are created using initial conditions different from those of the training samples.

In Figure 1 we plot the density fields and the particle distributions of three training samples, $(\Omega_m, A_s, \sigma_8) = (0.16, 2, 0.43), (0.26, 2.16, 0.72), (0.36, 2.0, 0.89)$. Obviously, the clustering strength increases when increasing Ω_m or A_s , making the structures more compact. In Figure 2 we plot the cosmologies of the training and testing samples, in the Ω_m - σ_8 space. In contrast to the Ω_m - A_s space, here we see a strong degeneracy between the two parameters. The prior distributions of these parameters may influence the performance of the CNN training and predicting, and this influence is unchecked in this work. The prior adopted in this work is uniformly distributed in Ω_m - A_s space which exhibits a strong degeneracy in Ω_m - σ_8 , which may not be optimal.

3. METHODOLOGY

One disadvantage of deep learning is that it is almost impossible to design an architecture from first principles for the task at hand. Furthermore, although a precise parameter estimation is achieved, it is difficult to say what spatial scale or features are the most relevant to predict the final cosmological parameters. Here we use a large number of filters for the initial spatial convolution, based on the belief that small scale structures contain abundant information and should be convolved by many filters to extract various features.

The input of the whole network is a 32^3 -voxel (i.e. $(64h^{-1} \text{ Mpc})^3$) subcube of the original density fields that is stored in a 128^3 -voxel cube. We do not feed the whole 128^3 voxel cube to the neural network based on three considerations.

1. To learn a larger cube the network should have more neurons or layers and thus its training becomes much more difficult and expensive.
2. Large cubes is challenging for the memory especially for off-the-shelf GPUs.
3. In this work we want to focus on scales of $\lesssim 50h^{-1} \text{ Mpc}$ ³. On larger scales, perturbation theory and 2-point statistics of dark matter distribution has been well studied.

In the next two layers, we group these small-scale features together to extract the large-scale features. It is fair to say that, in the end, we mainly use the information of structures on scales of $6 - 64 h^{-1} \text{ Mpc}$.

The default architecture we describe in this section is closer to that used in Mathuriya et al. (2018) than the one used in Ravanbakhsh et al. (2017). In the next section we also discuss the effect of changes to this default architecture.

The structure of our neural network is shown in Figure 3. It contains three convolution layers and three dense layers. In the next subsection we discuss the implementation details.

3.1. Convolution

CNNs networks are designed to be “shift/space invariance artificial neural networks”, having shared-weights architecture and translation invariance characteristics. They are especially suitable for analyzing images, videos, or any kind of structures with a large number of pixels/voxels and shift/space invariant properties.

The density field is fed to three convolutional layers. The inputs of these layers are one or many cubes. The convolutional kernels then convolve the inputs, and pass the results to the next layer.

The parameters in the convolutional kernels decide features to be extracted from the input data. They encode the prediction of cosmological parameters. For example, the first layer contains 32 3^2 -filters; this means that 32 features are extracted, by conducting dot product of the kernels of filters and the $(6 h^{-1} \text{ Mpc})^3$ subcubes of the data, with a stride of $2 h^{-1} \text{ Mpc}$. Clearly, the information extracted here belongs to the highly non-linear clustering region. The summation of the dot-products are transformed by the activation function (to have non-linear transformation in the network), for which we use rectified linear unit (ReLU), $f(x) = \max(x, 0)$. This simple form enables fast calculation of gradients and effectively suppresses over-fitting, and we accept it in the dense layers.

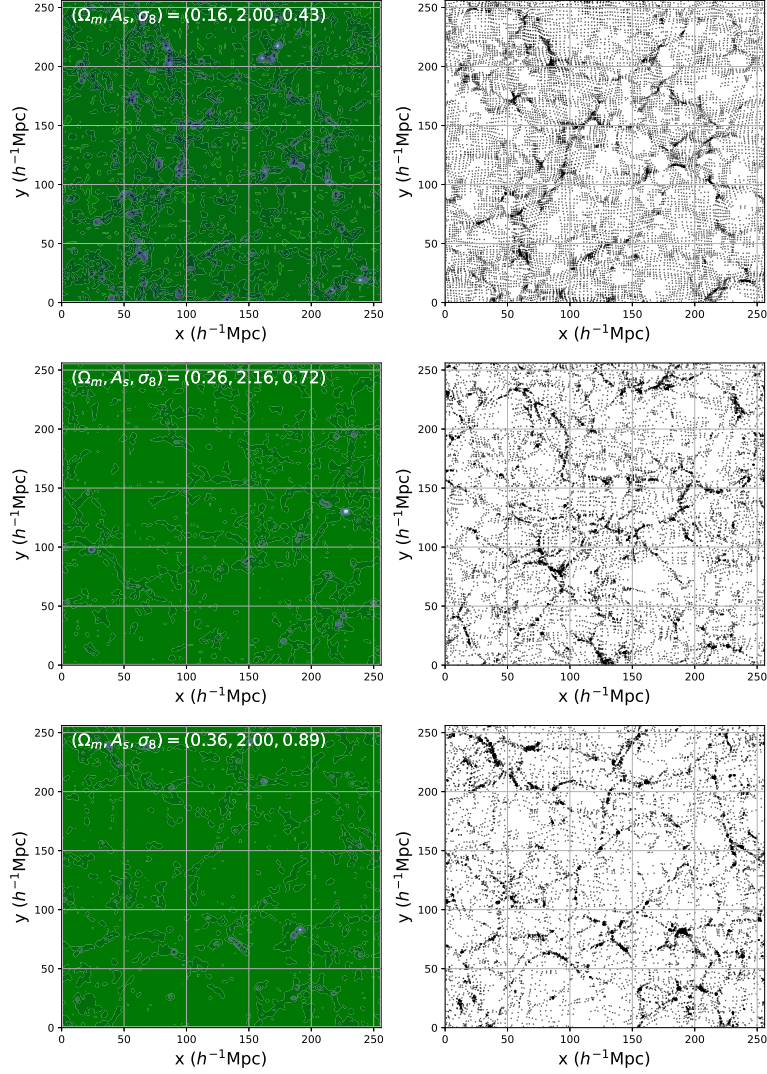


Figure 1. The density field (left) and particle distribution (right) in three cosmologies $(\Omega_m, A_s, \sigma_8) = (0.16, 2, 0.43), (0.26, 2.16, 0.72), (0.36, 2.0, 0.89)$, selected from the training sample. We plot the 2D distribution, with the third dimension restricted to a thin slice $0h^{-1}\text{Mpc} < z < 2h^{-1}\text{Mpc}$. The clustering strength is enhanced when increasing Ω_m or A_s , making the structures more “compact”. We train neural networks to build up connections between the density fields and their underlying cosmological parameters.

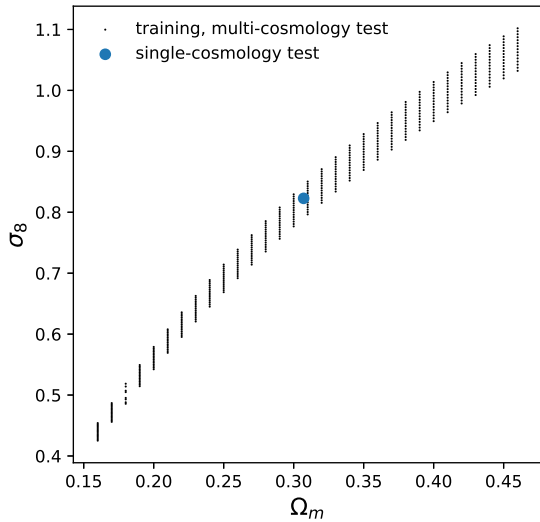


Figure 2. Ω_m and σ_8 values for the 465 training samples and single-cosmology test samples. The multi-cosmology test samples have exactly the same values of Ω_m and σ_8 as those in training samples.

In Figures 4,5, we show how the CNN works. Step by step, the features are extracted by the three layers, and become more and more condensed. Different filters identify different features. With a large number of filters we are able to perform a very comprehensive statistical analysis. The final outputs are 128 2^3 -voxel cubes. The Figures clearly show that two different cosmologies lead to significantly different outputs.

Notice that these cubes do contain enough information for the measuring of σ_8 . In the input of the CNN, all information is stored in the $(2 h^{-1}\text{Mpc})^3$ voxles. The first convolution is conducted using 32 3^3 kernels, thus, in the feature maps generated by it, each voxel contains information in a volume of $(6 h^{-1}\text{Mpc})^3$ (i.e., information within such a volume is mixed together after the first convolution). After a pooling and the second convolution, each voxel in the feature map then contains information spanning a volume of $(14 h^{-1}\text{Mpc})^3$, whose scale is already larger than $8 h^{-1}\text{Mpc}$. So, after another pooling, a third convolution, and a third pooling operation, the final 128 2^3 cubes is definitely capable for the probing of σ_8 ⁷.

⁷ This convince us that the final output of CNN has the ability of probing σ_8 , but since the CNN is too complicated for us to understand, we can only use tests justified (e.g., Figure 7 and 9) to check whether the information of σ_8 is really stored in these cubes.

The parameters of filters are tuned in the training process in a way that they can extract features which are closely related to the cosmological information. The optimized CNN is far more complicated than any traditional statistics (e.g., 2-point and 3-point statistics). This enables more comprehensive data mining.

3.2. Batch normalization and pooling

A batch normalization layer is placed before each convolution layer. Batch normalization is achieved through a normalization step that fixes the means and variances of each layer’s inputs. It was initially proposed to solve “internal covariate shift” problem⁸, and can also regularize the network such that it is easier to generalize. It has become a widely-accepted technique for improving the speed, performance and stability of the neural networks.

Results of each convolutional layer, are also passed to a “pooling” layer to decrease the sample size. Ravanbakhsh et al. (2017) suggests using averaging pooling for LSS data, so we adopt it as one of our default options of the network. However, for our architecture we find that max-pooling shows better performance.

3.3. Fully Connected Layers

Outputs of the final pooling are flattened and passed to three fully connected layers with 1024, 256 and 2 neurons, respectively. This system is a very complicated collection of non-linear mathematical functions, and is able to build up a connection between the features extracted by the CNN (in our case the 128 2^3 cubes) and the values of Ω_m and σ_8 . To suppress over-fitting, we have a 20% dropout layer placed before the dense layers.

We adopte MSE (mean squared error) as the loss function to describe the difference between the predictions of the whole neural network and the “true” values of (Ω_m, σ_8) . By default, we use the Adaptive Moment Estimation (Adam) optimization algorithm (Kingma & Ba 2014) to find the values of parameters (of the CNN and the fully connected layers) which minimize the loss function.

4. RESULTS

In this section we present the results of the neural network.

4.1. Convergence test

The leftmost column of Figure 6 shows the *learning curves* of two different runs using the default architecture. Plotted are the average of the predictions from the

⁸ The distributions of the internal layers’ inputs keep changing, causing problems in the training process.

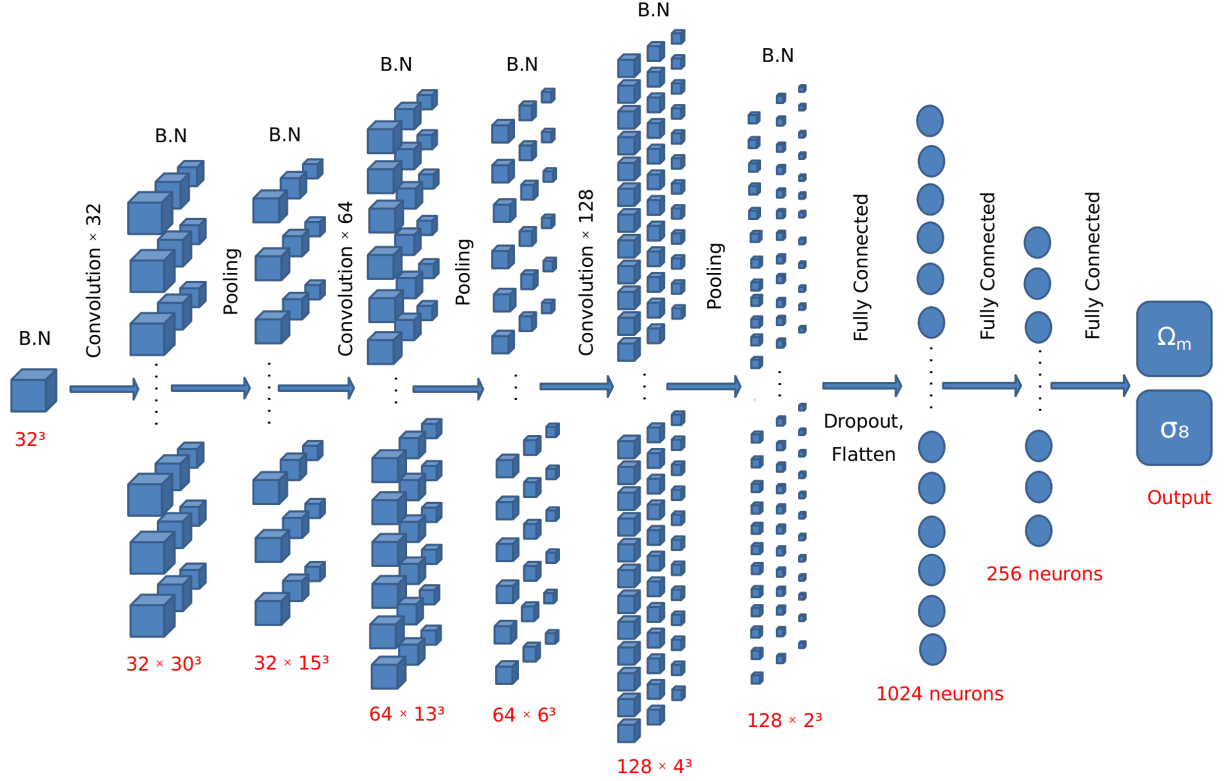


Figure 3. The architecture of our neural network. A cube having 32^3 voxels is fed to the network. The three convolution layers have 32, 64, 128 filters, respectively. Beside each convolution layer, a batch normalization layer is added before it to normalize the distribution (so that to enhance the stability), and a pooling layer is placed after it to decrease the size of the output. After that, we got 128×2^3 voxels containing the extracted features. They are then converted to a 1-d vector by the flatten layer, and passed to three dense layers with 1028, 24, 2 neurons, to output the final predictions of Ω_m and σ_8 .

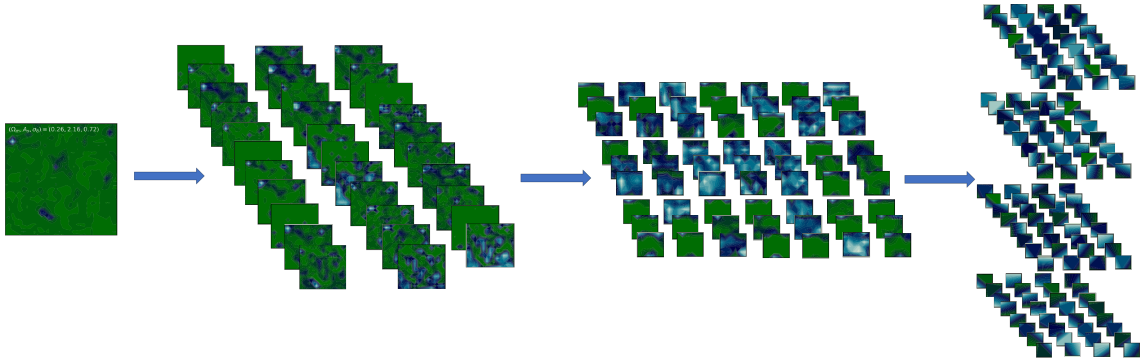


Figure 4. Layer-by-layer outputs of the CNN when fed by a sample with cosmology parameters $(\Omega_m, A_s, \sigma_8) = (0.26, 2.16, 0.72)$. The many filters, determined by the 896/55,360/221,312 trainable parameters in the three convolutions layers, can capture various types of features. The final outputs of the CNN is a set of 128×2^3 -boxes containing the most compressed features extracted from the data. They are passed to the dense layers (not plotted here) for parameter estimation.

500 single-cosmology samples. The two runs yield very different predictions at the early stage of training, while after ~ 200 epochs they start to converge and yield similar predictions (n training epoch means the whole training samples are fed to the network by n -th time). After 400 epochs, their predictions are basically the same.

Thanks to the lightness of our neural network the training is not significantly computationally expensive. It can finish within 1 week using the CPU of a personal computer. This makes it useful for many cosmologists who are interested in machine learning but not familiar with multiple-GPU implementations.

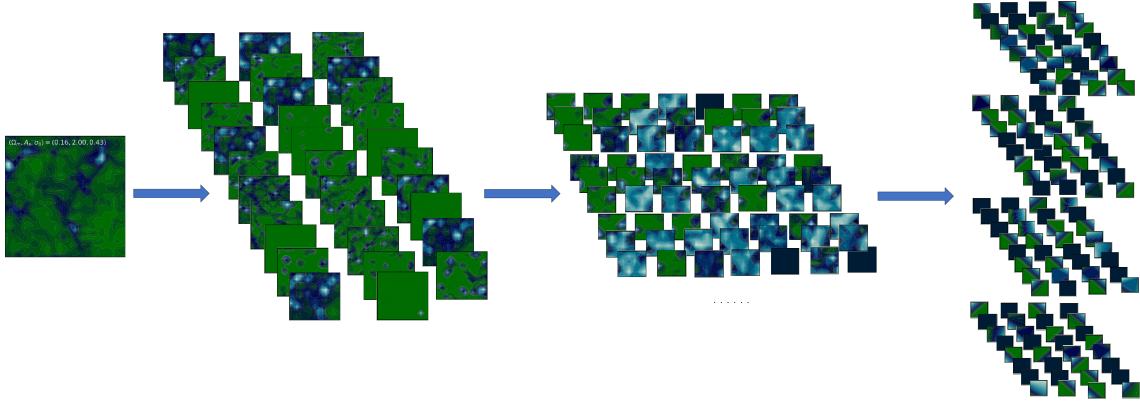


Figure 5. Same as Figure 4, except that for the case of $(\Omega_m, A_s, \sigma_8) = (0.26, 2.00, 0.43)$. The features extracted are significantly different from those in the cosmology $(\Omega_m, A_s, \sigma_8) = (0.26, 2.16, 0.72)$, making it possible to distinguish these two cosmologies.

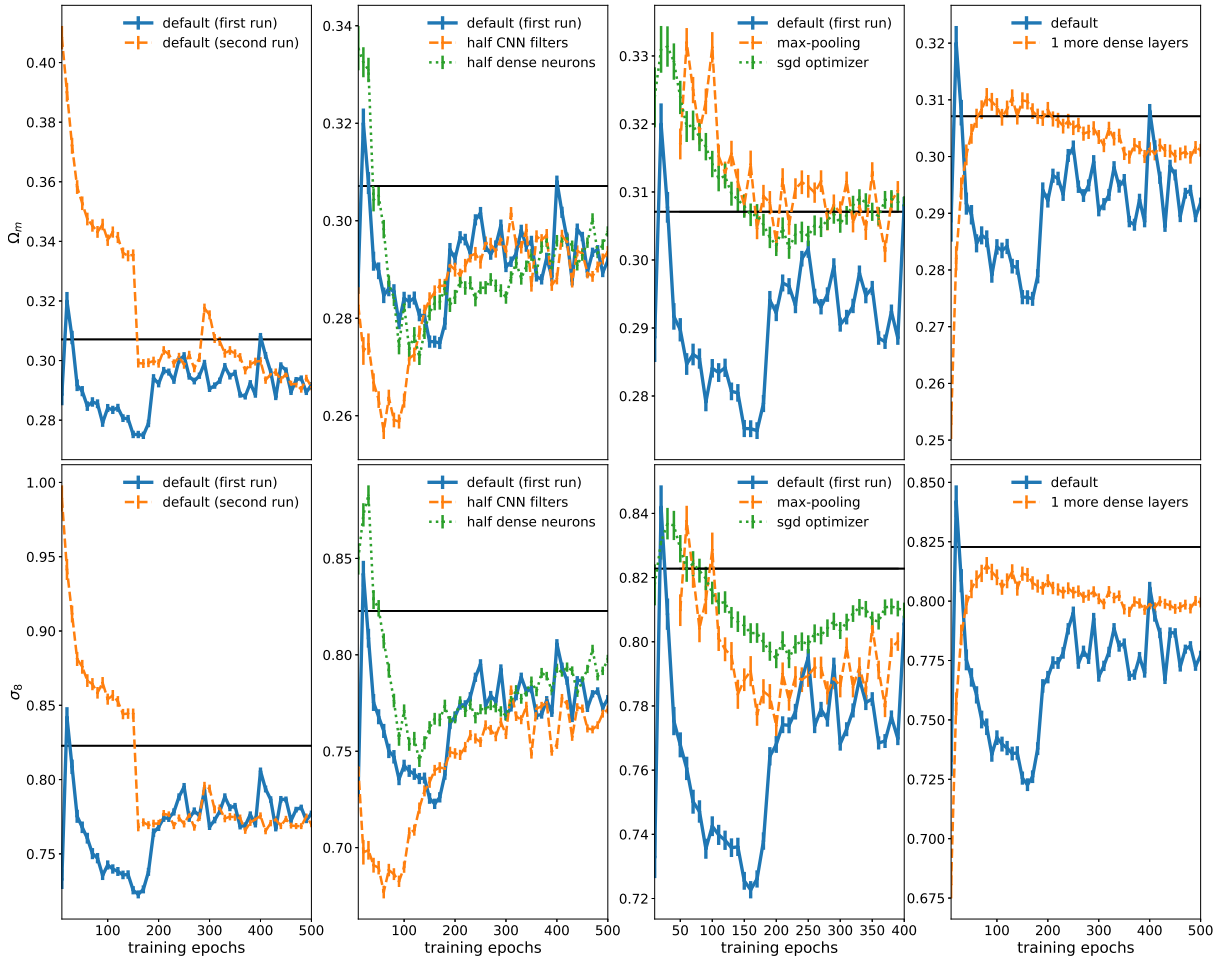


Figure 6. Learning curve using different architectures. First panel: two runs using the default options reaches convergence after 160 epochs. Second panel: decreasing the number of CNN filters or dense neurons by 50%, no significant change in the performance. Third panel: among our trials of different options, using max-pooling or SGD optimizer can notably enhance the performance. Fourth panel: an extra dense layer with 512 neurons are added before the final outputs to achieve a more accurate mapping from CNN outputs to the cosmological parameters. A good performance is detected at ≈ 80 epochs; more training epochs results in over-fitting.

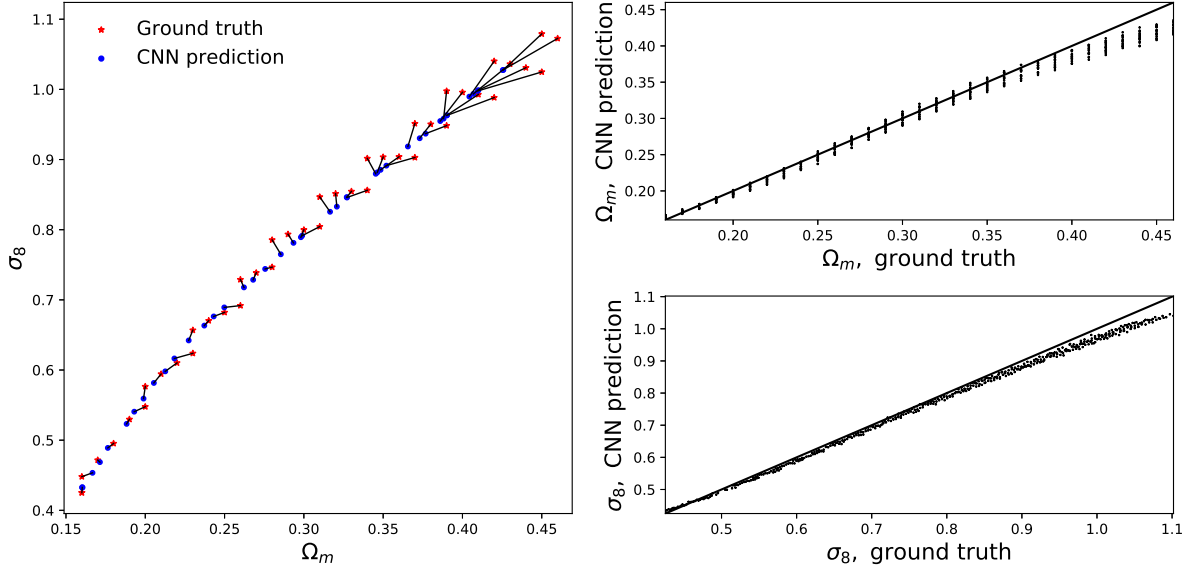


Figure 7. Test of a CNN architecture (sgd) on a multi-cosmology grid. There is a strong degeneracy between Ω_m and σ_8 . *Left panel:* Ground truth and CNN predictions of Ω_m and σ_8 , in the 2-d parameter space. The black lines show the difference between them. The bias is larger at the upper-right corner of the parameter space. *Right panels:* Ground truth and CNN predictions for Ω_m and σ_8 panels, respectively.

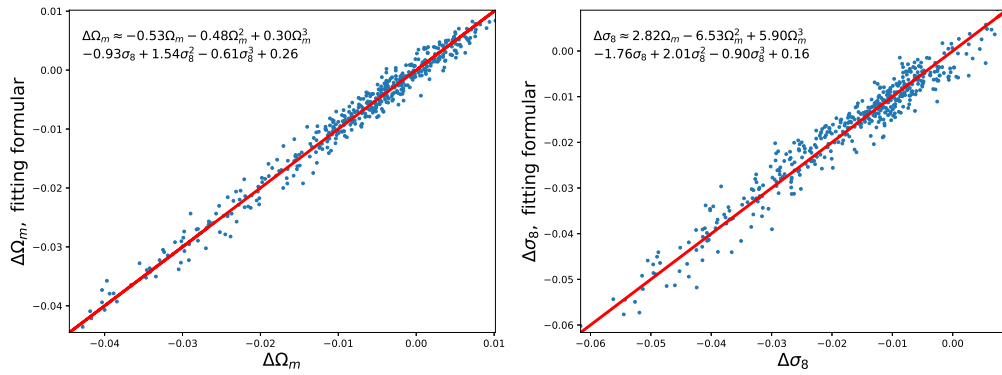


Figure 8. Distribution of the systematic bias in the CNN predicted Ω_m and σ_8 (denoted as $\Delta\Omega_m$ and $\Delta\sigma_8$). Very roughly, in the parameter space we studied, there is $|\Delta\Omega_m| \lesssim 0.03$ and $|\Delta\sigma_8| \lesssim 0.05$, with mean value of $\overline{|\Delta\Omega_m|} = 0.01$ and $\overline{|\Delta\sigma_8|} = 0.018$. In practice one can calibrate the results by subtract the systematic bias in the CNN predictions (e.g., using the fitting formula shown in the panels), making the final estimation unbiased.

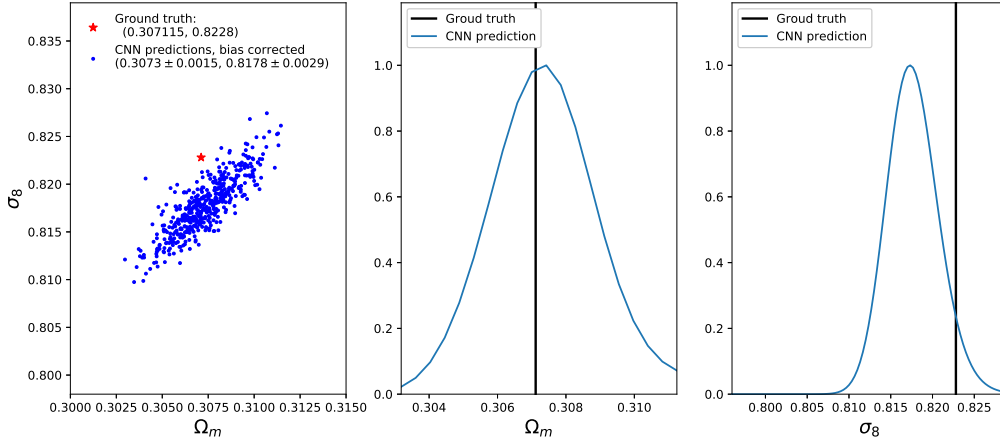


Figure 9. Test of a CNN architecture (sgd) on the single-cosmology samples. *Left panel:* Ground truth (red star) and CNN predictions (blue dots) of Ω_m and σ_8 , in the 2-d parameter space. The CNN well predicts the values of Ω_m , but has a bias in estimating σ_8 . *Middle and Right panels:* Likelihood distribution of Ω_m , σ_8 from the CNN predictions.

4.2. Different architecture

The middle columns of Figure 6 show some tests on the architecture choices.

We tuned the architecture by decreasing, either the number of filters in the convolutional layers, or the neurons in the dense layers, by a fraction of 50%; yet we find no significant change in their learning curves. We also tried doubling these numbers, and still obtain similar learning curves.

In the middle-right panel, we present results when we 1) use max-pooling instead of average-pooling; 2) use stochastic gradient (sgd) as the optimizer (the default optimizer is Adam). These changes slightly improve the performance (especially, decreasing the bias in the estimation of Ω_m).

4.3. Bias correction

We find a bias in the estimated parameters. This bias is smaller than the one reported by [Ravanbakhsh et al. \(2017\)](#), but larger than the apparently unbiased results of [Mathuriya et al. \(2018\)](#). In most cases, we under-estimate Ω_m by about 0.005 (less than 2%). While σ_8 is under-estimate by about 0.02 which is about 2.5%. Increasing the training epochs to 1,500 does not reduce this bias.

We do not have a definitive answer for the origin of this bias. One possibility is that it comes from the limited power of the dense layers in regressing the cosmological parameters from the 128 2^3 -voxel features. This hypothesis is supported by the fact that placing another 512-neuron layer after the 256-neuron layer, to improve the ability in mapping the many voxels to the param-

eters, the bias is obviously decreased (see rightmost panel of Figure 6).

To have a better understanding of the bias, we plot its parameter-dependence in Figure 7. We find a clear trend of increasing bias at larger values Ω_m or σ_8 . This trend is again consistent with the results in [Ravanbakhsh et al. \(2017\)](#).

Adding more layers/neurons in the dense layers to further decrease the bias goes against of our objective of having a simple and light convolutional network. Instead, we opt for a simpler (and possibly more accurate) treatment by deducting the bias based on a polynomial regression⁹. Figure 8 shows that the biases can be well estimated using a 3-rd order polynomial as functions of Ω_m and σ_8 .

The fitting formula (here a high order polynomial) may become complicated when there are 6-7 model parameters, however implementing it is always simple and straightforward. Also, its complexity is not comparable with that of the neural network.

4.4. Cosmological constraint

Figure 9 shows the final constraints derived from the 500 single-cosmology samples, where the bias has been subtracted based on the polynomial regression. To avoid self-correction, the regression is derived using the multi-cosmology samples, which have no overlapping from the single-cosmology samples.

⁹ A polynomial regression may sound arbitrary, but in principle it has no intrinsic difference from a mapping using dense layers.

We find the CNN accurately predicts the parameters as

$$\Omega_m = 0.3073 \pm 0.0015, \sigma_8 = 0.8178 \pm 0.0029. \quad (2)$$

They are statistically consistent with the ground truth (0.3071, 0.8228). We find the prediction of σ_8 still suffers from a $\approx 1\sigma$ bias; this can be overcome by performing a more precise bias-estimation based on larger amount of samples (e.g. a point-by-point correction on the grid)¹⁰.

The statistical error of Ω_m is 6 times smaller than the Planck 2015 TT,TE,EE+lowP+lensing constraint, 4 times smaller than Planck+BAO+JLA+ H_0 constraint (Ade et al. 2016)¹¹. Having derived this result from a $(256 h^{-1} \text{ Mpc})^3$, $2 h^{-1} \text{ Mpc}$ resolution sample shows the great potential of using neural network to estimate cosmological parameters from the LSS.

One caveat is that the variance of parameters may depend on the value of parameters. In practice, one can generate several sets of mocks on different positions of the parameter space to estimate this effect. Then the dependence on the whole parameter space can be modeled via interpolation.

Compared with the results of Ravanbakhsh et al. (2017), the errors of our predicted Ω_m and σ_8 are 5 and 2 times smaller, while our constraints are achieved using simulation samples with 8 times smaller box-size and 64 times smaller number-of-particles¹².

As a comparison with traditional methods, Ravanbakhsh et al. (2017) conducted a power spectrum analysis, and found the error of its predicted Ω_m is 2.6 times larger than their CNN error, hence 13 times larger than our CNN error. If we assume the accuracy of power spectrum analysis scales with the square-root of sample volume, then our CNN is ≈ 25 times more precise than a power spectrum analysis in predicting Ω_m .

To better understand the potential of the CNN we also made a comparison with the 2-point correlation function (2pcf) analysis results. The 2pcf constraints on parameters are derived by measuring the shape and amplitude of the 2pcfs using samples in the many cosmologies, to

build an emulator. We find CNN constraints on Ω_m/σ_8 are 3.5/2.3 and 19/11 times more precise than the 2pcf analysis using the clustering range of 0-130 and 10-130 $h^{-1} \text{ Mpc}$, respectively. Notice that the 2pcf analysis is very ideal, since in realistic analysis we usually use the clustering region $s \gtrsim 30 h^{-1} \text{ Mpc}$, while the amplitude information, being affected by many systematics, can not be easily utilized.

4.5. Error tolerance

So far we only apply the neural network to *ideal* datasets – density fields regularly sampled in a 3-d grid based on the dark matter particles. In reality, the data obtained in observations contain many sources of systematics. Here, we quantify how this noise affects the performance of the neural network.

The ET (error tolerance) tests are presented in Figure 10. For simplicity, in these tests we only use *one* 128^3 -voxel sample, generated using $(\Omega_m, \sigma_8)=(0.26, 0.69)$. We split the grid into 64 32^3 -voxel subgrids to obtain 64 sets of estimated parameters. Adding different kinds of noise into the subgrids, and feed them to the neural network to predict parameters. When a certain kind of noise was added, we check whether the estimations are changed, and get some understandings about the effect of noise.

In summary, we find that:

- A smoothing of the sample¹³ can lead to disastrous effect. Even a 1% smoothing shifts the estimation by $\approx 2\sigma$. A 3% smoothing doubles the shifts and also doubles the statistical scattering
- In contrast, the performance of the neural network is very robust to missing voxels. We mask 1 or 4^3 voxels in each of the 32^3 -subgrid (by setting their values to 0), and find the predicted results almost unchanged. This ET ability is helpful, since in real observations there are always many masked regions.
- The performance is not significantly improved if we conduct data enhancement (DE) via rotation and reflection. The number of the 3d subgrids can be increased by as much as 48 times after DE. No significant improvement in the predictions is detected if we feed the 48-times more samples to the neural network.

¹⁰ The bias on σ_8 , being on level of 1σ , is not statistically significant and worth further studies. One can use multiple such realizations, or a larger realization, to achieve better estimations.

¹¹ The comparison is not “very suitable” since 1) Our analysis is based on noise-free simulations; 2) We do not include the systematical uncertainties; 3) CMB and LSS are very different types of observations. This comparison is just for illustrative purpose to enable readers easily understand that the results are really precise and the CNN analysis of LSS data is promising.

¹² If we simply assume that the information scales with the number of particles, then our CNN is 40/16 times better in predicting Ω_m/σ_8 compared with Ravanbakhsh et al. (2017).

¹³ Our smoothing means that each voxel is replaced by a weighted sum of itself and its six nearest neighbors. Different types of smoothing can have different effect and should be tested individually.

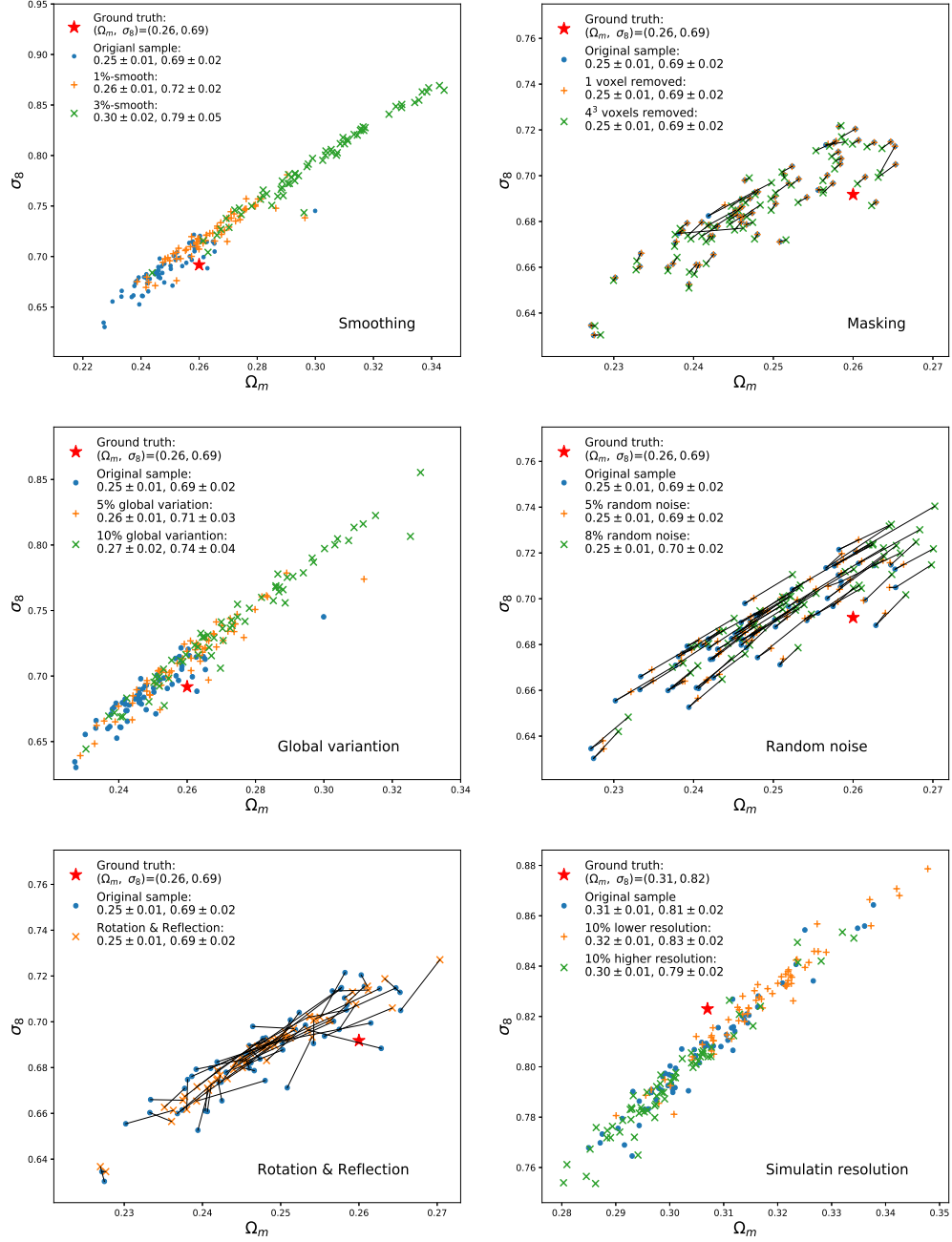


Figure 10. Error-tolerance tests. A 3% smoothing or 10% global variation leads to considerable change in the predicted results ($\sim 2\sigma$ shift in central values, $\sim 100\%$ enlarged errors). 1% smoothing, 5% global variation, and 10% change in the simulation's resolution mildly affect the prediction ($\sim 1\sigma$ shift in central values, errors unchanged). Other cases, including the 1 or 4³ voxels removal, 5% or 8% random noise addition, rotation and reflection, does not affect the results at all.

Table 1. Comparison between this work and [Ravanbakhsh et al. \(2017\)](#)

	Method	Training sample	Relative error of $(\Omega_m, \sigma_8)^a$
Ravanbakhsh et al. (Ravanbakhsh et al. 2017)	CNN	450 simulations $(512 h^{-1}\text{Mpc})^3$, 512^3 particles	(0.028, 0.012)
Ravanbakhsh et al. (Ravanbakhsh et al. 2017)	Power spectrum	450 simulations $(512 h^{-1}\text{Mpc})^3$, 512^3 particles	(0.072, 0.013)
This work	CNN	465 simulations $(256 h^{-1}\text{Mpc})^3$, 128^3 particles	(0.0048, 0.0053)
This work	2pcf, $s \in (0, 130)h^{-1}\text{Mpc}$	465 simulations $(256 h^{-1}\text{Mpc})^3$, 128^3 particles	(0.017, 0.012)
This work	2pcf, $s \in (10, 130)h^{-1}\text{Mpc}$	465 simulations $(256 h^{-1}\text{Mpc})^3$, 128^3 particles	(0.1, 0.06)

^aDefined as $\Delta y/y$ (y stands for Ω_m, σ_8) where Δy includes both the statistical error and bias

- The predictions are very robust to Gaussian noise. In this test, all voxels are multiplied by a Gaussian random variable with a standard deviation of 5% or 10%. The central values and errors remain unchanged.
- If we introduce a 5% or 10% *global* variation (rescaling) of the density field (linearly increased from 0% at $x = 0$ to the maximal value at $x = 256h^{-1}\text{Mpc}$), notable change appears in the predicted results. Thus, when analyzing observational data, one should be careful about the factors which can globally change the survey properties in a large area.
- In case that we feed the neural network using samples produced in 10% lower/higher resolution (decreasing/increasing the number of simulation particles by 10%), the central values are mildly shifted ($\sim 1\sigma$).

The above tests have not previously been performed in [Ravanbakhsh et al. \(2017\)](#); [Mathuriya et al. \(2018\)](#), so this constitutes a first check of these systematics. The results justify that the neural network analysis is not, as some suspected, significantly sensitive to even tiny systematics variations. Although these tests are oversimplified compared with those that should be done when dealing with real observational data, the tests enable us to have some preliminary understanding of the influence of the systematics effects.

When handling real observational data, an observational artifact can be overcome in two ways. 1) Designing a neural network that is robust to it. This can be done by modeling the systematics by several parameters, and allowing them to run over a wide range in the training sample, so that the neural network is adaptable to a wide range of systematics parameters. This can handle those systematics which are not well understood. 2) For well-known systematics, one can simply add it into the training sample, so that its effect is considered by the neural network in the training process.

5. CONCLUDING REMARKS

We used a deep convolutional neural network to estimate cosmological parameters from simulated dark matter distributions. The simulations are 128^3 -voxel, $(256 h^{-1} \text{Mpc})^3$ cubes of the dark matter density contrast field. The neural network, designed to have three convolution layers, three dense layers, including batch normalization and pooling layers, builds up a connection from the field to the cosmological parameters. It is able to yield accurate prediction of the cosmological parameters after $\sim 200 - 300$ epochs of training. We

also studied some variations on the architecture to test its convergence and overall performance.

In the estimated parameters, we find a persistent bias that can not be resolved by increasing the training epochs. We believe that this bias arises from the limited power of the dense layers, which are responsible for mapping the outputs of the convolution to the cosmological parameters. Using more sophisticated dense layers, or simply applying a subtraction based on polynomial regression, the bias can be suppressed. We also tested the error-tolerance abilities of the neural network, including the abilities against smoothing, masking, random noise, global variation, rotation, reflection and resolution.

The robustness tests are still preliminary and only enable us have some basic understanding about the influence of the systematics. Once one uses dark matter distributions to populate galaxies, the inclusion of more complicated systematics would be required due to the complexity of the problem. This needs to be explored in future analysis. Also, considering that the size of the sample used in the test is relatively small, we can only obtain some basic understanding of the systematics at this point.

We obtain precise estimations, with statistical scattering of $\delta\Omega_m=0.0015$ and $\delta\sigma_8=0.0029$, from the neural network. The statistical error of Ω_m is 6 and 4 times smaller than the Planck and Planck+ext constraints presented in [Ade et al. \(2016\)](#). We conclude that deep neural networks are very promising in estimating cosmological parameters from the LSS.

The persistent bias in the prediction of our neural network would be the biggest caveat limiting the power of the technique. The bias was also detected in the work of [Ravanbakhsh et al. \(2017\)](#), yet the authors did not provide a strategy to overcome it. It seems that the bias is greatly reduced if one uses a more complex network architecture with seven convolutional layers and 128^3 voxels as an input ([Mathuriya et al. 2018](#)).

The approach that we develop to correct the bias is a simple subtraction based on polynomial regression. This is not completely satisfactory and future work should aim to address this problem, i.e. measuring how it depends on the architecture parameters. This will allow us to design better architectures with a smaller bias, and conducting more concrete tests based on larger training samples. This study is a required prerequisite to conduct a reliable, comprehensive analysis of LSS using deep learning.

On the physical side there are at least many directions for future work.

1. In this simple work, we haven't consider the role of redshift space distortion (RSD) in the param-

- ter estimation. We tend to believe that the RSDs, which creates more cosmological dependent features in the matter distribution, should lead to better parameter estimation. We will test this supposition in forth-coming works.
2. In the case of a survey covering a $(512 h^{-1} \text{ Mpc})^3$ or $(1 h^{-1} \text{ Gpc})^3$ volume of density field, one can further decrease the statistical error by 3 or 8 times. In that case the bias and error tolerance (to systematics) of the neural network would be essentially important. Lightcone effect, selection function, galaxy bias, redshift errors, or even baryonic effects, should be tested in certain circumstances.
 3. The resolution of our input sample, $2 h^{-1} \text{ Mpc}$, is a bit high when considering the current and near-future spectroscopic surveys, which have low comoving number densities. So it will be necessary to apply the method to lower-resolution, more realistic galaxy samples. In the next step, we will apply it to dark matter halo samples, and see whether the neural network is still able to achieve precise parameter estimation in such circumstances.
 4. While in this work we only consider the predictions of Ω_m and σ_8 , in general the CNN can be used to probe any cosmology or astrophysical parameters which can affect the large scale structure. An incomplete list include the parameters related with

the Hubble constant (Riess et al. 2016; Wang et al. 2017), dark energy equation of state and its time dependence (Miao et al. 2011; Zhao & Wang 2018; Li et al. 2019a), gravity (Sotiriou & Faraoni 2010; Tsujikawa 2011; Abbott et al. 2017; Zheng et al. 2018; Li et al. 2019b; Zhang 2019), galaxy formation and evolution (White & Rees 1978; Dressler 1980), and so on.

We thank Kwan-Chuen Chan, Cheng Cheng, Zhiqi Huang, Yin Li, Guangcong Wang and Xin Wang for helpful discussions. XDL thanks Ziyong Wu and Xiaolin Luo for kind helps. We acknowledge the use of *Kunlun* cluster located in School of Physics and Astronomy, Sun Yat-Sen University.

XDL acknowledges the supported from NSFC grant (No. 11803094), the Science and Technology Program of Guangzhou, China (No. 202002030360). J.E. F-R acknowledges support from COLCIENCIAS Contract No. 287-2016, Project 1204-712-50459. CGS acknowledges financial support from the National Research Foundation (NRF; #2017R1D1A1B03034900, #2017R1A2B2004644 and #2017R1A4A1015178). ZL was supported by the Project for New faculty of Shanghai JiaoTong University (AF0720053), the National Science Foundation of China (No. 11533006, 11433001) and the National Basic Research Program of China (973 Program 2015CB857000).

REFERENCES

- Abbott, B. P., Abbott, R., Abbott, T. D., et al. 2017, *Nature*, 551, 85
- Ade, P. A., Aghanim, N., Arnaud, M., et al. 2016, *Astronomy & Astrophysics*, 594, A13
- Alam, S., Ata, M., Bailey, S., et al. 2017, *Monthly Notices of the Royal Astronomical Society*, 470, 2617
- Alcock, C., & Paczyński, B. 1979, *Nature*, 281, 358
- Anderson, L., Aubourg, E., Bailey, S., et al. 2012, *Monthly Notices of the Royal Astronomical Society*, 427, 3435
- Anderson, L., Aubourg, É., Bailey, S., et al. 2014, *Monthly Notices of the Royal Astronomical Society*, 441, 24
- Ballinger, W., Peacock, J., & Heavens, A. 1996, *Monthly Notices of the Royal Astronomical Society*, 282, 877
- Bardeen, J. M., Bond, J. R., Kaiser, N., & Szalay, A. S. 1986, *ApJ*, 304, 15
- Berger, P., & Stein, G. 2019, *Mon. Not. Roy. Astron. Soc.*, 482, 2861
- Beutler, F., Blake, C., Colless, M., et al. 2011, *Monthly Notices of the Royal Astronomical Society*, 416, 3017
- Beutler, F., Seo, H.-J., Saito, S., et al. 2016, *Monthly Notices of the Royal Astronomical Society*, 466, 2242
- Blake, C., & Glazebrook, K. 2003, *ApJ*, 594, 665
- Blake, C., Glazebrook, K., Davis, T. M., et al. 2011a, *Monthly Notices of the Royal Astronomical Society*, 418, 1725
- Blake, C., Brough, S., Colless, M., et al. 2011b, *Monthly Notices of the Royal Astronomical Society*, 415, 2876
- Caldeira, J., Wu, W. L. K., Nord, B., et al. 2018, *arXiv:1810.01483*
- Carleo, G., Cirac, I., Cranmer, K., et al. 2019, *arXiv:1903.10563*
- Chardin, J., Uhlich, G., Aubert, D., et al. 2019, *arXiv:1905.06958*
- Chuang, C.-H., Pellejero-Ibanez, M., Rodríguez-Torres, S., et al. 2017, *Monthly Notices of the Royal Astronomical Society*, 471, 2370
- Colless, M., et al. 2003, *arXiv:astro-ph/0306581*

- de Lapparent, V., Geller, M. J., & Huchra, J. P. 1986, *ApJL*, 302, L1
- Dreissigacker, C., Sharma, R., Messenger, C., Zhao, R., & Prix, R. 2019, *Phys. Rev.*, D100, 044009
- Dressler, A. 1980, *ApJ*, 236, 351
- Eisenstein, D. J., Hu, W., & Tegmark, M. 1998, *Astrophys. J.*, 504, L57
- Eisenstein, D. J., et al. 2005, *Astrophys. J.*, 633, 560
- Fang, F., Forero-Romero, J., Rossi, G., Li, X.-D., & Feng, L.-L. 2019, *Mon. Not. Roy. Astron. Soc.*, 485, 5276
- Fluri, J., Kacprzak, T., Lucchi, A., et al. 2019, *arXiv:1906.03156*
- Gebhard, T. D., Kilbertus, N., Harry, I., & Schlkopf, B. 2019
- Gillet, N., Mesinger, A., Greig, B., Liu, A., & Ucci, G. 2019, *Mon. Not. Roy. Astron. Soc.*, 484, 282
- Gupta, A., Matilla, J. M. Z., Hsu, D., & Haiman, Z. 2018, *Phys. Rev.*, D97, 103515
- Guzzo, L., Scodeggio, M., Garilli, B., et al. 2014, *A&A*, 566, A108
- Hassan, S., Andrianomena, S., & Doughty, C. 2019a, *arXiv:1907.07787*
- Hassan, S., Liu, A., Kohn, S., & La Plante, P. 2019b, *Mon. Not. Roy. Astron. Soc.*, 483, 2524
- He, S., Li, Y., Feng, Y., et al. 2019, *Proc. Nat. Acad. Sci.*, 116, 13825
- Huchra, J. P., Macri, L. M., Masters, K. L., et al. 2012, *ApJS*, 199, 26
- Ishida, E. E. O., et al. 2019, *Mon. Not. Roy. Astron. Soc.*, 483, 2
- Jeffrey, N., Lanusse, F., Lahav, O., & Starck, J.-L. 2019, *arXiv:1908.00543*
- Jennings, W. D., Watkinson, C. A., Abdalla, F. B., & McEwen, J. D. 2019, *Mon. Not. Roy. Astron. Soc.*, 483, 2907
- Kaiser, N. 1987, *Monthly Notices of the Royal Astronomical Society*, 227, 1
- Kingma, D. P., & Ba, J. 2014, *arXiv e-prints*, *arXiv:1412.6980*
- Klypin, A., Yepes, G., Gottlöber, S., Prada, F., & Hess, S. 2016, *Monthly Notices of the Royal Astronomical Society*, 457, 4340
- Koda, J., Blake, C., Beutler, F., Kazin, E., & Marin, F. 2016, *Mon. Not. Roy. Astron. Soc.*, 459, 2118
- La Plante, P., & Ntampaka, M. 2018, *Astrophys. J.*, 810, 110
- Lavaux, G., & Wandelt, B. D. 2012, *The Astrophysical Journal*, 754, 109
- Li, H.-L., Feng, L., Zhang, J.-F., & Zhang, X. 2019a, *Science China Physics, Mechanics, and Astronomy*, 62, 120411
- Li, J., Che, Z.-C., & Huang, Q.-G. 2019b, *Science China Physics, Mechanics, and Astronomy*, 62, 110421
- Li, S.-Y., Li, Y.-L., & Zhang, T.-J. 2019a, *arXiv:1907.00568*
- Li, X.-D., Miao, H., Wang, X., et al. 2019b, *Astrophys. J.*, 875, 92
- Li, X.-D., Park, C., Forero-Romero, J. E., & Kim, J. 2014, *ApJ*, 796, 137
- Li, X.-D., Park, C., Forero-Romero, J. E., & Kim, J. 2014, *The Astrophysical Journal*, 796, 137
- Li, X.-D., Park, C., Sabiu, C. G., & Kim, J. 2015, *Monthly Notices of the Royal Astronomical Society*, 450, 807
- Li, X.-D., Park, C., Sabiu, C. G., et al. 2017, *Astrophys. J.*, 844, 91
- Li, X.-D., Sabiu, C. G., Park, C., et al. 2018, *Astrophys. J.*, 856, 88
- Lochner, M., McEwen, J. D., Peiris, H. V., Lahav, O., & Winter, M. K. 2016, *Astrophys. J. Suppl.*, 225, 31
- Lucie-Smith, L., Peiris, H. V., & Pontzen, A. 2019, *arXiv:1906.06339*
- Lucie-Smith, L., Peiris, H. V., Pontzen, A., & Lochner, M. 2018, *Mon. Not. Roy. Astron. Soc.*, 479, 3405
- Marinoni, C., & Buzzi, A. 2010, *Nature*, 468, 539
- Mathuriya, A., et al. 2018, *arXiv:1808.04728*
- Mehta, P., Bukov, M., Wang, C.-H., et al. 2019, *Phys. Rept.*, 810, 1
- Merten, J., Giocoli, C., Baldi, M., et al. 2019, *Mon. Not. Roy. Astron. Soc.*, 487, 104
- Miao, L., Xiao-Dong, L., Shuang, W., & Yi, W. 2011, *Communications in Theoretical Physics*, 56, 525
- Mishra, A., Reddy, P., & Nigam, R. 2019, *arXiv:1908.04682*
- Modi, C., Feng, Y., & Seljak, U. 2018, *JCAP*, 1810, 028
- Moss, A. 2018, *arXiv:1810.06441*
- Muthukrishna, D., Parkinson, D., & Tucker, B. 2019, *arXiv:1903.02557*
- Mnchmeyer, M., & Smith, K. M. 2019, *arXiv:1905.05846*
- Ntampaka, M., et al. 2019, *arXiv:1902.10159*
- Peebles, P. J. E., & Ratra, B. 2003, *Reviews of modern physics*, 75, 559
- Peel, A., Lalande, F., Starck, J.-L., et al. 2019, *Phys. Rev.*, D100, 023508
- Percival, W. J., Cole, S., Eisenstein, D. J., et al. 2007, *Mon. Not. Roy. Astron. Soc.*, 381, 1053
- Perlmutter, S., Aldering, G., Goldhaber, G., et al. 1999, *The Astrophysical Journal*, 517, 565
- Perraudin, N., Defferrard, M., Kacprzak, T., & Sgier, R. 2019, *Astron. Comput.*, 27, 130

- Pfeffer, D. N., Breyse, P. C., & Stein, G. 2019, arXiv:1905.10376
- Ramanah, D. K., Charnock, T., & Lavaux, G. 2019a, *Phys. Rev.*, D100, 043515
- Ramanah, D. K., Lavaux, G., Jasche, J., & Wandelt, B. D. 2019b, *Astron. Astrophys.*, 621, A69
- Ravanbakhsh, S., Oliva, J., Fromenteau, S., et al. 2017, arXiv:1711.02033
- Riess, A. G., Filippenko, A. V., Challis, P., et al. 1998, *The Astronomical Journal*, 116, 1009
- Riess, A. G., Macri, L. M., Hoffmann, S. L., et al. 2016, *ApJ*, 826, 56
- Rodriguez, A. C., Kacprzak, T., Lucchi, A., et al. 2018, *Comput. Astrophys. Cosmol.*, 5, 4
- Ross, A. J., Samushia, L., Howlett, C., et al. 2015, *Monthly Notices of the Royal Astronomical Society*, 449, 835
- Ryden, B. 1995, arXiv preprint astro-ph/9506028
- Sabiu, C. G., Hoyle, B., Kim, J., & Li, X.-D. 2019, *ApJS*, 242, 29
- Sabiu, C. G., Mota, D. F., Llinares, C., & Park, C. 2016, *A&A*, 592, A38
- Samushia, L., Reid, B. A., White, M., et al. 2014, *Monthly Notices of the Royal Astronomical Society*, 439, 3504
- Sánchez, A. G., Scóccola, C., Ross, A., et al. 2012, *Monthly Notices of the Royal Astronomical Society*, 425, 415
- Sánchez, A. G., Kazin, E. A., Beutler, F., et al. 2013, *Monthly Notices of the Royal Astronomical Society*, 433, 1202
- Sánchez, A. G., Scoccamarro, R., Crocce, M., et al. 2016, *Monthly Notices of the Royal Astronomical Society*, 464, 1640
- Schmelzle, J., Lucchi, A., Kacprzak, T., et al. 2017, arXiv:1707.05167
- Seo, H.-J., & Eisenstein, D. J. 2003, *ApJ*, 598, 720
- Slepian, Z., Eisenstein, D. J., Brownstein, J. R., et al. 2017, *MNRAS*, 469, 1738
- Sotiriou, T. P., & Faraoni, V. 2010, *Reviews of Modern Physics*, 82, 451
- Springer, O. M., Ofek, E. O., Weiss, Y., & Merten, J. 2018, arXiv:1808.07491
- Tassev, S., Zaldarriaga, M., & Eisenstein, D. 2013, *JCAP*, 1306, 036
- Tegmark, M., Blanton, M. R., Strauss, M. A., et al. 2004, *ApJ*, 606, 702
- Tewes, M., Kuntzer, T., Nakajima, R., et al. 2019, *Astron. Astrophys.*, 621, A36
- Trster, T., Ferguson, C., Harnois-Draps, J., & McCarthy, I. G. 2019, *Mon. Not. Roy. Astron. Soc.*, 487, L24
- Tsujikawa, S. 2011, *Astrophysics and Space Science Library*, Vol. 370, *Dark Energy: Investigation and Modeling*, ed. S. Matarrese, M. Colpi, V. Gorini, & U. Moschella, 331
- Wang, Y., Xu, L., & Zhao, G.-B. 2017, *ApJ*, 849, 84
- Weinberg, D. H., Mortonson, M. J., Eisenstein, D. J., et al. 2013, *Physics reports*, 530, 87
- Weinberg, S. 1989, *Reviews of modern physics*, 61, 1
- White, S. D. M., & Rees, M. J. 1978, *MNRAS*, 183, 341
- York, D. G., Adelman, J., Anderson Jr, J. E., et al. 2000, *The Astronomical Journal*, 120, 1579
- Zhang, X. 2019, *Science China Physics, Mechanics, and Astronomy*, 62, 110431
- Zhang, X., Wang, Y., Zhang, W., et al. 2019a, arXiv:1902.05965
- Zhang, Z., Gu, G., Wang, X., et al. 2019b, *Astrophys. J.*, 878, 137
- Zhao, Z., & Wang, S. 2018, *Science China Physics, Mechanics, and Astronomy*, 61, 39811
- Zheng, H., Wei, L.-F., Wen, H., & Li, F.-Y. 2018, *Science China Physics, Mechanics, and Astronomy*, 61, 79531